

Research article

Xiaohu Mi^a, Yuyang Wang^a, Rui Li^a, Mengtao Sun^{*}, Zhenglong Zhang^{*} and Hairong Zheng

Multiple surface plasmon resonances enhanced nonlinear optical microscopy

<https://doi.org/10.1515/nanoph-2018-0231>

Received December 26, 2018; revised January 22, 2019; accepted January 23, 2019

Abstract: The nonlinear optical microscopies of coherent two-photon excited fluorescence and anti-Stokes Raman scattering are strongly enhanced by multiple surface plasmon resonances (MSPRs). The Au@Ag nanorods presented strong MSPRs peaks at 800 and 400 nm, and can enhance nonlinear optical microscopy at fundamental and double frequencies, respectively. A two-dimensional (2D) material of g-C₃N₄ is employed to study the plasmon-enhanced nonlinear optical microscopy by the femtosecond laser. The electric analysis reveals that the MSPRs of the Au@Ag nanorod can significantly enhance the signals of two-photon excited fluorescence and anti-Stokes Raman scattering by up to the orders of 10⁴ and 10¹⁶, respectively. The results demonstrate the great advantages of plasmon-enhanced nonlinear optical microscopy for the optical analysis on 2D materials, thus providing a new adventure for increasing the optical resolutions of nonlinear optical microscopy.

Keywords: TPEF; CARS; MSPRs; Au@Ag nanorods; surface plasmon.

1 Introduction

By means of nonlinear interactions between light and matter, nonlinear optical microscopy has become an important tool to produce sensitive optical images and spectroscopy, including coherent and incoherent processes [1]. The coherent microscopes of coherent anti-Stokes Raman scattering (CARS) [2–4], second-harmonic generation [5–7] and stimulated Raman scattering [8] generate nonlinear optical signals, whose phases are strictly stipulated by many aspects, such as the phase of excitation light and the steric distribution of target molecules. The nonlinear coherent microscopy is ground on the simultaneous scattering of two or more photons, and the coherent signal intensity is proportional to M^2 , where M is the concentration of radiating molecules. For incoherent microscopies, such as the two-photon excited fluorescence (TPEF) microscopy [9–11], they generate nonlinear optical signals, whose phases are random, and the intensity is proportional to M . Compared with the confocal Raman/fluorescence microscopy, the TPEF microscopy can penetrate deeper in thick samples. Normally, the nonlinear interactions of TPEF and CARS only occur in specific intrinsic biological molecules [12] or two-dimensional (2D) materials [13], which provide optical imaging and spectroscopy without the need for exogenous stains, especially for *in vivo* applications.

The optical nonlinearity originating from the material properties of interacting media are inherently weak, especially for CARS. As the coherent Raman signal is proportional to $N(N-1)$, where N is the number of molecules [14], the coherence enhancement decreases with the decrease of N and vanishes for a single molecule. Thus, measuring the coherent Raman imaging at nanoscale is a highly challenging task because of the smaller number of molecules. The nanoscale confinement of optical fields using plasmonic nanostructures provides an effective strategy for enhancing the Raman/fluorescence spectroscopy [15]. The surface plasmon arises from the collective coherent oscillation of free electrons at an optical frequency, which can significantly enhance both the incoherent and coherent nonlinear processes, including the plasmon-enhanced CARS [16], second-harmonic generation [17, 18], hyper-Raman

^aXiaohu Mi, Yuyang Wang and Rui Li: These authors contributed equally to this work.

***Corresponding authors: Mengtao Sun**, Center for Green Innovation, School of Mathematics and Physics, Beijing Advanced Innovation Center for Materials Genome Engineering, Beijing Key Laboratory for Magneto-Photoelectrical Composite and Interface Science, University of Science and Technology Beijing, Beijing, China, e-mail: mengtaosun@ustb.edu.cn. <https://orcid.org/0000-0002-8153-2679>; and **Zhenglong Zhang**, School of Physics and Information Technology, Shaanxi Normal University, Xi'an, China, e-mail: zlzhang@snnu.edu.cn

Xiaohu Mi, Yuyang Wang and Hairong Zheng: School of Physics and Information Technology, Shaanxi Normal University, Xi'an, China

Rui Li: School of Physics, Dalian University of Technology, Dalian, China

scattering [19] and TPEF [20]. Moreover, the plasmonic Au/Ag nanostructures are also capable of generating inherent nonlinear optical processes [21], including second-harmonic generation [22, 23]; excited-state absorption [24], multiphoton, third-harmonic generation [25, 26]; four-wave mixing [27] and photoluminescence (PL) [28]. Given that just one plasmon resonance (fundamental or double) frequency can be excited for near-field enhancement, the enhancement factor is quite small for the normal plasmonic nanoparticles. Therefore, finding a special nanostructure is very important as this can enhance nonlinear optical signals at fundamental and double frequencies, i.e. multiple surface plasmon resonances (MSPRs).

In this paper, the Au@Ag nanorods are synthesized in order to demonstrate the MSPRs at the fundamental and double frequencies of 800 and 400 nm, respectively. By employing a 2D material of $g\text{-C}_3\text{N}_4$, we demonstrate that the nonlinear optical microscopy of TPEF and two-photon CARS can be significantly enhanced by the MSPRs. The simulations strongly support the experimental observations. The results also indicate that a selected Au@Ag nanorod can totally enhance the two-photon CARS of 2D materials, and provide a simple method using the MSPRs to enhance nonlinear optical microscopy.

2 Experiments

2.1 Synthesis of the Au@Ag nanorods

All reagents were used without further purification, and deionized water was used in the experiment. HAuCl_4 , Hexadecyltrimethylammonium bromide (CTAB), sodium borohydride (NaBH_4), silver nitrate (AgNO_3) and sodium oleate (NaOL) were purchased from Sigma Aldrich (Shanghai, China). Hydrochloric acid (HCl), Sodium hydroxide (NaOH), ascorbic acid and glycine were purchased from Sinopharm Chemical Reagent Co., Ltd. (Shanghai, China).

The Au nanorods were synthesized using an improved seed-mediated wet-chemical method [29]. The solution of Au seed was made by adding 0.25 ml of HAuCl_4 (0.01 M) into the 9.75 ml of CTAB (0.1 M), to which 0.048 ml of NaBH_4 (0.1 M) aqueous was added while stirring at 1200 rpm for 1 min. For the growth solution, 1.234 g NaOL and 0.7 g CTAB were added into 50 ml water, while stirring at 70°C, after which 0.72 ml of AgNO_3 (0.01 M) was injected into the solution while the temperature was reduced to 30°C. After 15 min, 2.5 ml of HAuCl_4 (0.01 M) was added to the solution while stirring for 90 min. Then, 1.8 ml of HCl (1 M) was added to adjust the pH, after which 0.08 ml of ascorbic

acid (0.1 M) and 0.04 ml seeds solution were added and maintained at a temperature of 30°C for 12 h.

The Au@Ag nanorods were synthesized on the ground above the Au nanorods [30]. The Au nanorods were re-dispersed in 20 ml of CTAB (0.1 M) solution, after which 17.8 ml of glycine buffer solution (0.4 M) and 1.2 ml of AgNO_3 (0.01 M) were added while stirring. Then, 0.6 ml of ascorbic acid (0.1 M) were added into the solution while stirring for 3 hours. The prepared Au@Ag nanorods were dispersed onto the $g\text{-C}_3\text{N}_4$ layer on glass by spin coating.

2.2 Characterization and measurements

The scanning electron microscope (SEM) images were obtained by a FEI-Nova Nano SEM 450 (Hillsboro, OR, USA) operating at a voltage of 10 kV, and the transmission electron microscopy (TEM) images were collected from the JEOL 2100 (Akishima, Tokyo, Japan) operating at an acceleration voltage of 200 kV. The mappings were obtained on field-emission transmission electron microscope (FE-TEM) at a voltage of 200 kV. The UV-visible extinction spectra were measured by using a Perkin Elmer Lambda 950 spectrometer (Waltham, MA, USA). The detailed instruments and measurements are described in previous works [13]. In short, the TPEF and CARS images are measured with the nonlinear optical microscopy. A femtosecond mode-locked Ti:Sapphire laser of 800 nm (80 fs and 80 MHz) was employed in this nonlinear optical microscopy system.

2.3 Simulations

The extinction spectrum and electric field distribution were simulated by finite element method with COMSOL Multiphysics. The geometric parameters of the Au@Ag nanorods and the direction of polarization of the incident light were set. The inner nanostructure comprised an Au nanorod with a length of 100 nm and a diameter of 12 nm. A 10 nm silver layer shell was coated on each Au nanorod. The nanorods were located in the x-y plane, and a plane wave as the incident light was set in a direction with an angle of θ .

3 Results and discussion

The plasmon-enhanced nonlinear optical microscopy of $g\text{-C}_3\text{N}_4$ was studied by using the MSPRs of the Au@Ag nanorods (Figure 1A). The SEM images of the plasmonic Au@Ag nanorods shown in Figure 1B–D demonstrate that the Au@Ag nanorods are successfully synthesized, and a silver shell is coated onto each Au nanorod

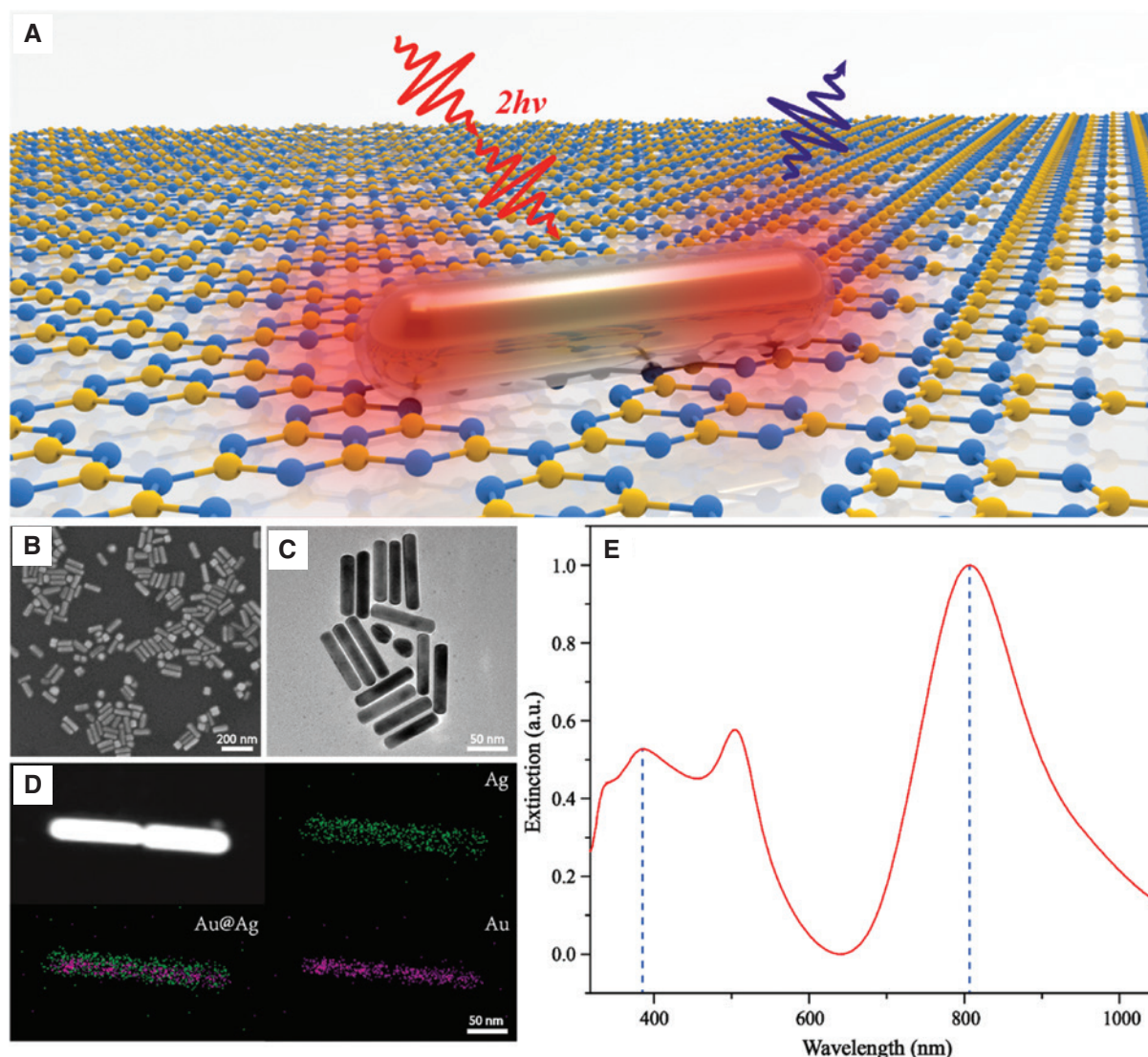


Figure 1: Characterization and optical properties of Au@Ag nanorods.

(A) Plasmon-enhanced nonlinear optical microscopy of $g\text{-C}_3\text{N}_4$ by the Au@Ag nanorods. (B and C) The SEM and TEM images of the Au@Ag nanorods, and (D) the elemental mapping images of the two Au@Ag nanorods. (E) UV-visible spectra of the chemically synthesized Au@Ag nanorods.

with a thickness of around 10 nm. Compared with the Au nanorods, the resonance peaks at 910 and 520 nm indicate a blue shift to 800 and 500 nm for the Au@Ag nanorods, and a new resonance peak at 400 nm can be obtained (Figure S1).

The plasmon-enhanced TPEF of $g\text{-C}_3\text{N}_4$ covered with the Au@Ag nanorods was first studied (Figure 2). According to the absorption and PL spectra of $g\text{-C}_3\text{N}_4$ shown in Figure 2B, a strong extinction peak can be observed around 400 nm, which matches the fundamental frequency at 800 nm of the incident light. The TPEF images of $g\text{-C}_3\text{N}_4$ without (Figure 2C) and with (Figure 2D) the Au@Ag nanorods were obtained by 800 nm excitation. By

using strong MSPRs at 800 and 400 nm, the TPEF can be strongly enhanced via the Au@Ag nanorods covering on the $g\text{-C}_3\text{N}_4$ surface.

In order to decrease the PL intensity and promote the Raman efficiency, a defecting $g\text{-C}_3\text{N}_4$ by N vacancy on tris-s-triazine was used to measure the plasmon-enhanced CARS. As shown in Figure 3, the TPEF and CARS images are obtained from a defecting $g\text{-C}_3\text{N}_4$ without (A–D) and with (E–H) the Au@Ag nanorods. The TPEF images demonstrate that the PL intensity is significantly decreased (Figure 3B). However, the two-photon CARS image is too weak to be observed (Figure 3C). To enhance the intensity and resolutions of TPEF and CARS, the

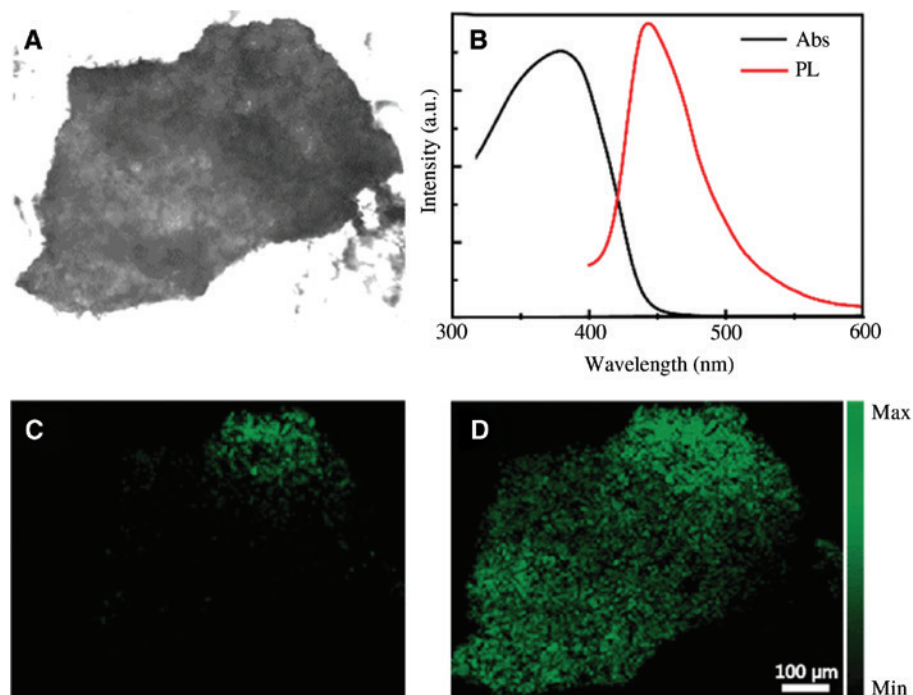


Figure 2: Optical characterization of $g\text{-C}_3\text{N}_4$.

(A) The bright field optical image of $g\text{-C}_3\text{N}_4$. (B) The absorption and PL spectra of $g\text{-C}_3\text{N}_4$. (C) The TPEF and (D) plasmon-enhanced TPEF of $g\text{-C}_3\text{N}_4$ without and with the Au@Ag nanorods, respectively.

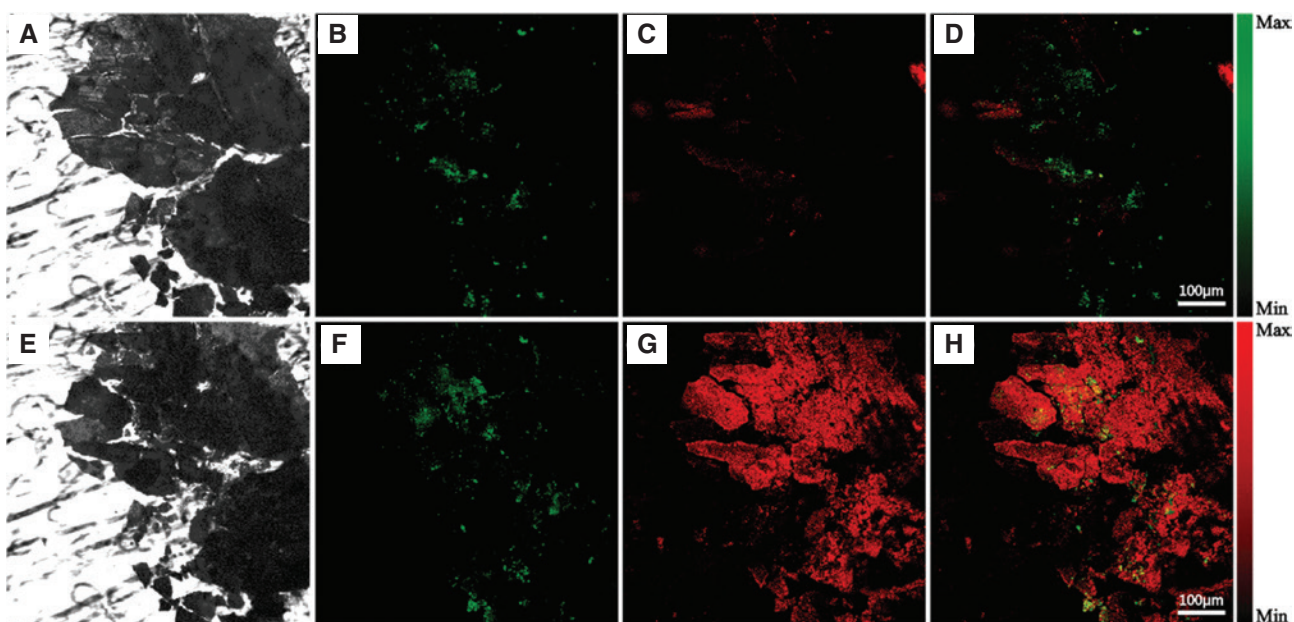


Figure 3: Optical characterization of plasmon-enhanced $g\text{-C}_3\text{N}_4$.

(A) The bright field optical image of defective $g\text{-C}_3\text{N}_4$. (B) The TPEF (C) CARS and (D) merged images of $g\text{-C}_3\text{N}_4$. (E) The bright field optical image of the defective $g\text{-C}_3\text{N}_4$ with the Au@Ag nanorods. (F) The plasmon-enhanced TPEF, (G) CARS and (H) merged images of defected $g\text{-C}_3\text{N}_4$.

Au@Ag nanorods were covered on the defected $g\text{-C}_3\text{N}_4$ (Figure 3E). Due to the extremely weak PL intensity of $g\text{-C}_3\text{N}_4$, no obvious enhanced signals can be observed

from the enhanced TPEF image in Figure 3F. However, the CARS signals are extremely enhanced by the Au@Ag nanorods because of a very strong nonlinear electric

magnetic field enhancement (Figure 3G). Compared with the merged images (Figure 3D and H), the CARS signals are dominantly observed from the merged plasmon-enhanced TPEF and CARS images.

In order to understand the above results, the simulated electric analyses for TPEF and CARS were done by FEM (Figure 4). We found that the MSPR models can be controlled by the angle of incident light. By scanning the nanorod length and shell thickness, the geometrical parameters of the Au@Ag nanorod are well optimized to match the MSPR peaks of 800 and 400 nm, which agrees with the experimental geometry (Figure S2). As shown in the extinction spectrum in Figure 4B, the strongest SPR peaks at 800 nm and 400 nm result from the excitation along the long (0°) and short (90°) axes, respectively. When the incident angle is 0° , a longitudinal mode is excited, and the strong electric field enhancements can be found at the terminals of the Au@Ag nanorods (Figure 4C). When the incident angle is 90° , a horizontal mode is excited, and a significant enhancement of electric field on both short sides of the Au@Ag nanorod can be observed for the resonance mode at the wavelength of 400 nm (Figure 4D).

The electric field enhancement factor (EF) of TPEF and the two-photon CARS are respectively written as [31]

$$EF_{TPEF} = \left| \frac{E(\omega)}{E_0(\omega)} \right|^2 \left| \frac{E(\omega_s)}{E_0(\omega_s)} \right|^4 = |g(\omega)|^2 |g(\omega_s)|^4, \quad (1)$$

$$EF_{tpCARS} = \left| \frac{E(\omega)}{E_0(\omega)} \right|^8 \left| \frac{E(\omega_s)}{E_0(\omega_s)} \right|^4 = |g(\omega)|^8 |g(\omega_s)|^4, \quad (2)$$

where ω and ω_s are the frequencies of incident light and scattered light, respectively, and $|g|$ is the local electric field enhancement around the probe molecules. According to the experimental system, we investigated the incident angles depending on the extinction spectrum of the Au@Ag nanorods and the EF of the TPEF and CARS. Figure 4B shows the extinction spectra of the Au@Ag nanorod structure with incident angles varying from 0° to 90° . The intensity of the resonance peak at 800 nm is increased with the decrease of the resonance peak at 400 nm. The extinction spectrum well matches the experimental extinction spectrum when the incident angle is 30° , which can be attributed to the average effect in experiments. According to Equations (1) and (2), we calculated the EF of TPEF and CARS of the Au@Ag nanorod by the electric field enhancement at 800 nm and 400 nm. The incident

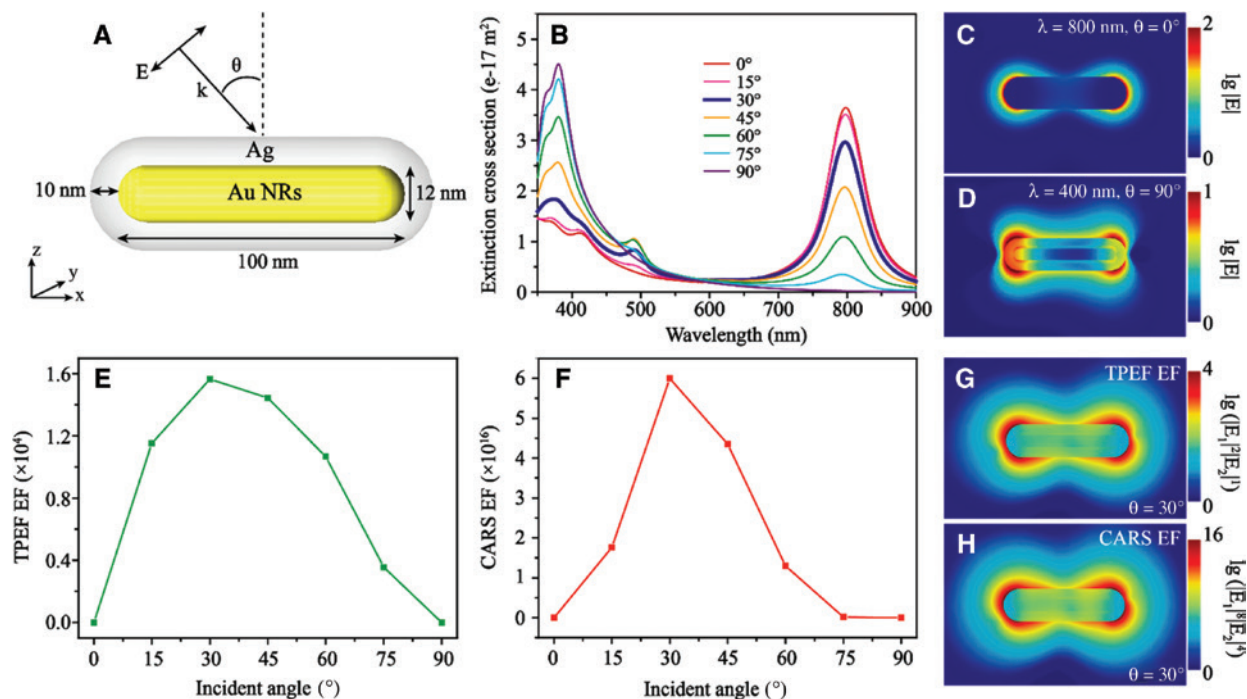


Figure 4: Nonlinear plasmonic enhancement of the Au@Ag nanorods.

(A) Schematic of simulation model of the Au@Ag nanorods. (B) Incident angle-dependent extinction spectra from 0° to 90° with an increment of 15° . (C and D) Distributions of the electric field intensity of the Au@Ag nanorods with excitations of 800 and 400 nm, respectively. (E and F) The incident angle-dependent enhancement of the TPEF and CARS, respectively, and more detailed calculated results shown in the supporting information of Figure S6. (G and H) The respective distributions of the enhanced TPEF and CARS.

angle-dependent electric field enhancement for plasmon-enhanced TPEF and CARS demonstrate that the angle of the strongest plasmon enhancements is 30° , which is up to 10^4 and 10^{16} , respectively (Figure 4E and F). As can be seen on the distribution for the TPEF and CARS enhancements shown in Figure 4G and H, a strong electric field enhancement can be observed at the end and both sides of the Au@Ag nanorods, because the symmetry is broken by the oblique incidence and some multipolar resonance mode can be excited. The electric field distributions of other incident angles are shown in the supporting information (Figures S3–5). Therefore, the EF of the TPEF and two-photon CARS can reach the maximum of 1.6×10^4 and 6×10^{16} with an incident angle of 30° , respectively, which are larger than those of the normal fluorescence and CARS, respectively.

4 Conclusion

Using the chemically synthesized Au@Ag nanorods, the plasmon-enhanced nonlinear optical microscopy of the TPEF and two-photon CARS were revealed by the MSPRs. The nonlinear optical signals of $g\text{-C}_3\text{N}_4$ is significantly enhanced due to the double-enhanced frequencies at 800 and 400 nm. Moreover, the CARS signals can be clearly distinguished from the merge nonlinear optical images. The simulation results strongly support the experimental observations, and the calculated enhancements reach up to 10^4 and 10^{16} for the TPEF and two-photon CARS, respectively. The new method of using the MSPRs not only enhance the nonlinear optical signal intensity but also has the potential to improve imaging accuracy and resolution in future applications.

Acknowledgments: This work was supported by the National Natural Science Foundation of China (Grant Nos. 91436102 and 11374353), the Fundamental Research Funds for the Central Universities in USTB and SNNU (GK201701008), the National Basic Research Program of China (Grant No. 2016YFA0200802) and the 111 Project (Grant No. B170003).

References

- [1] Wei M, Freudiger CW, Lu S, Xie XS. Coherent nonlinear optical imaging: beyond fluorescence microscopy. *Annu Rev Phys Chem* 2011;62:507–30.
- [2] Evans CL, Xie XS. Coherent Anti-Stokes Raman scattering microscopy: chemical imaging for biology and medicine. *Annu Rev Anal Chem* 2008;1:883–909.
- [3] Evans CL, Potma EO, Puoris'haag M, et al. Chemical imaging of tissue *in vivo* with video-rate coherent anti-Stokes Raman scattering microscopy. *Proc Natl Acad Sci USA* 2005;102:16807–12.
- [4] Hellerer T, Axang C, Brackmann C, et al. Monitoring of lipid storage in *Caenorhabditis elegans* using coherent anti-Stokes Raman scattering (CARS) microscopy. *Proc Natl Acad Sci USA* 2007;104:14658–63.
- [5] Chen X, Nadiarynkh O, Plotnikov S, Campagnola PJ. Second harmonic generation microscopy for quantitative analysis of collagen fibrillar structure. *Nat Protoc* 2012;7:654–69.
- [6] Franken PA, Hill AE, Peters CW, Weinreich G. Generation of optical harmonics. *Phys Rev Lett* 1961;7:118–19.
- [7] Shen YR. Surface properties probed by second-harmonic and sum-frequency generation. *Nature* 1989;337:519–25.
- [8] Freudiger CW, Min W, Saar BG, et al. Label-free biomedical imaging with high sensitivity by stimulated Raman scattering microscopy. *Science* 2008;322:1857–61.
- [9] Denk W, Strickler JH, Webb WW. Two-photon laser scanning fluorescence microscopy. *Science* 1990;248:73–76.
- [10] Vinegoni C, Feruglio PF, Brand C, et al. Measurement of drug-target engagement in live cells by two-photon fluorescence anisotropy imaging. *Nat Protoc* 2017;12:1472–97.
- [11] Svoboda K, Yasuda R. Principles of two-photon excitation microscopy and its applications to neuroscience. *Neuron* 2006;50:823–39.
- [12] Li R, Wang X, Zhou Y, et al. Advances in nonlinear optical microscopy for biophotonics. *J Nanophoton* 2018;12:1.
- [13] Li R, Zhang Y, Xu X, et al. Optical characterizations of two-dimensional materials using nonlinear optical microscopies of CARS, TPEF, and SHG. *Nanophotonics* 2018;7:873–81.
- [14] Petrov GI, Arora R, Yakovlev VV, et al. Comparison of coherent and spontaneous Raman microspectroscopies for noninvasive detection of single bacterial endospores. *Proc Natl Acad Sci USA* 2007;104:7776–9.
- [15] Deka G, Sun CK, Fujita K, Chu SW. Nonlinear plasmonic imaging techniques and their biological applications. *Nanophotonics* 2017;6:31–49.
- [16] Ichimura T, Hayazawa N, Hashimoto M, Inouye Y, Kawata S. Tip-enhanced coherent anti-Stokes Raman scattering for vibrational nanoimaging. *Phys Rev Lett* 2004;92:220801.
- [17] Campagnola PJ, Clark HA, Mohler WA, Lewis A, Loew LM. Second-harmonic imaging microscopy of living cells. *J Biomed Opt* 2001;6:277–86.
- [18] Chen CK, Castro ARB, Shen YR. Surface-enhanced second-harmonic generation. *Phys Rev Lett* 1981;46:145–48.
- [19] Golab J, Sprague JR, Carron KT, Schatz GC, Duyn RPV. A surface enhanced hyper-Raman scattering study of pyridine adsorbed onto silver: experiment and theory. *J Chem Phys* 1988;88:7942–51.
- [20] Sanchez EJ, Novotny L, Xie X. Near-field fluorescence microscopy based on two-photon excitation with metal tip. *Phys Rev Lett* 1999;82:4014–17.
- [21] Kauranen M, Zayats AV. Nonlinear plasmonics. *Nat Photon* 2012;6:737–48.
- [22] Butet J, Duboisset J, Bachelier G, et al. Optical second harmonic generation of single metallic nanoparticles embedded in a homogeneous medium. *Nano Lett* 2010;10:1717–21.

- [23] Butet J, Brevet PF, Martin OJF. Optical second harmonic generation in plasmonic nanostructures: from fundamental principles to advanced applications. *ACS Nano* 2015;9:10545–62.
- [24] Chen T, Chen S, Zhou J, Liang D, Chen X, Huang Y. Transient extinction microscopy of gold nanorods as spectrally orthogonal labels in live cells. *Nanoscale* 2014;6:10536–39.
- [25] Jung Y, Tong L, Tanaudommongkon A, Cheng J, Yang C. *In vitro* and *in vivo* nonlinear optical imaging of silicon nanowires. *Nano Lett* 2009;9:2440–44.
- [26] Lippitz M, Dijk MAV, Orrit M. Third-harmonic generation from single gold nanoparticles. *Nano Lett* 2005;5:799–802.
- [27] Renger J, Quidant R, Hulst NV, Novotny L. Surface-enhanced nonlinear four-wave mixing. *Phys Rev Lett* 2010;104:046803.
- [28] He H, Xie C, Ren J. Nonbleaching fluorescence of gold nanoparticles and its applications in cancer cell imaging. *Anal Chem* 2008;80:5951–7.
- [29] Ye X, Zheng C, Chen J, Gao Y, Murray CB. Using binary surfactant mixtures to simultaneously improve the dimensional tunability and monodispersity in the seeded growth of gold nanorods. *Nano Lett* 2013;13:765–71.
- [30] Contreras-Caceres R, Dawson C, Formanek P, et al. Polymers as templates for Au and Au@Ag bimetallic nanorods: UV-Vis and surface enhanced Raman spectroscopy. *Chem Mater* 2013;25:158–69.
- [31] Voronine DV, Zhang Z, Sokolov AV, Scully MO. Surface-enhanced FAST CARS: en route to quantum nano-biophotonics. *Nanophotonics* 2018;7:523.

Supplementary Material: The online version of this article offers supplementary material (<https://doi.org/10.1515/nanoph-2018-0231>).